Probing Catalytic Solid-Liquid Interfaces by Attenuated Total Reflection Infrared Spectroscopy: Adsorption of Carboxylic Acids on Alumina and Titania

by **Davide Ferri**, **Thomas Bürgi**, and **Alfons Baiker***

Laboratory of Technical Chemistry, Swiss Federal Institute of Technology, ETH-Hönggerberg, CH-8093 Zurich (tel.: +41 (0)1 632 31 53; fax: +41 (0)1 632 11 63; e-mail: baiker@tech.chem.ethz.ch)

Dedicated to Professor *Dieter Seebach* on the occasion of his 65th birthday

The adsorption of carboxylic acids (formic, acetic, and pyruvic acid) from corresponding solutions in CH_2Cl_2 solvent on Al_2O_3 and TiO_2 thin films has been studied by attenuated total reflection infrared spectroscopy. The metal-oxide films were vapor-deposited on a Ge internal reflection element, which was mounted into a specially designed flow cell. The system allowed *in situ* monitoring of the processes occurring at the solid-liquid interface. The metal-oxide films were characterized by X-ray photoelectron spectroscopy, ellipsometry, and atomic force microscopy. Formic acid and acetic acid adsorbed predominantly as bridging species on alumina surfaces. Adsorbed free acids were not observed under a flow of neat solvent. Based on the position of the $\nu_{AS}(COO)$ and of the keto-group stretching vibration of the pyruvate ion, pyruvic acid is proposed to coordinate to the Al_2O_3 surface in a monodentate fashion, whereas, on TiO_2, a bidentate species is preferred. Comparison of the adsorption behavior on the vapor-deposited alumina film and on an α-Al_2O_3 layer deposited from a water suspension of the corresponding metal-oxide powder indicated that pyruvic acid adsorbs in a similar mode, irrespective of the metal-oxide deposition technique.

Introduction. – Solid-liquid interfaces play fundamental roles in nature and technology. Many processes crucial for life occur at such interfaces and technical applications range from corrosion, tribology, electrochemistry over environmental chemistry to heterogeneous catalysis. Our knowledge of such important processes relies on techniques that probe the respective interfaces. The growing awareness that an interface may be quite different under working conditions than under conditions far away from these, has fostered the development of *in situ* methods. In the field of heterogeneous catalysis, important insight can be gained by monitoring the respective catalytic interface at work.

Vibrational spectroscopy is ideally suited to probe interfaces [1][2]. A vibrational spectrum contains detailed structural information of the adsorbate layer such as interaction mode between surface and adsorbate, orientation of the adsorbate and intermolecular interactions within the adsorbate layer. Furthermore, infrared radiation is noninvasive. The advances in vibrational spectroscopy of interfaces in the past few years went along with progress in instrumentation and data processing. Furthermore, the information contained in the measured spectra can now be read in more detail through comparison with calculations. The availability of sophisticated *ab initio* quantum-chemical programs and fast computers makes it possible to simulate spectra with predictive accuracy.

In heterogeneous catalysis research, IR spectroscopy has recently been extensively used to study catalytic solid-gas interfaces *in situ* [3]. In contrast, catalytic solid-liquid interfaces have hardly been studied *in situ*, by vibrational spectroscopy or by any other technique, despite their importance. An exception to this is represented by the work in electrochemistry, where vibrational spectroscopy has been used for many years [4]. The presence of a dense bulk medium, usually a solvent, represents the major experimental challenge and calls for techniques that can probe the interface selectively. Potential methods are sum-frequency generation (SFG) [5] and polarization-modulation IR reflection absorption spectroscopy (PM-IRRAS) [6], which are insensitive to bulk media, or surface enhanced *Raman* spectroscopy (SERS) [7], where signals are preferentially generated at the interface, due to an enhanced electric field at rough metal surfaces.

We have recently used attenuated total reflection (ATR) IR spectroscopy [8] to probe the solid-liquid interface of supported Pt and Pd catalysts in contact with organic solvents [9–14]. Here, we describe the adsorption of monocarboxylic acids on alumina and titania surfaces. Both materials are metal oxides extensively used in several practical applications ranging from microelectronics and optics to ceramics, catalysis, and pollution abatement. The adsorption of carboxylic acids, such as salicylic [15–17], benzoic [16–19], oxalic [16][20–22], and dicarboxylic acids [22], has been in the focus of several ATR-IR studies. Being oxidation products of alcohols, they belong to the class of volatile organic compounds, and, as such, their abatement is relevant for the environment [23][24]. Mineral surfaces can store and release ionic surfactants and possess practical importance in chemical and photocatalytic reactions [25–27]. Adsorption of carboxylic acids on wet surfaces has also received growing interest in the field of soil chemistry, in particular due to environmental implications. Organic materials constitute the predominant adsorbed species on metal oxides, and the presence of functional groups facilitates their bonding to surfaces. On adsorption, they can dramatically change the properties of the metal oxide, for example, by inhibiting the adsorption of metal ions or by decreasing the resistance of the metal oxide to corrosion by abstracting the metal centers from the bulk [28]. Formic acid and its derivatives play a pivotal role in catalytic C_1-chemistry [29].

Here, we report the adsorption of formic acid, acetic acid, and pyruvic acid on alumina and titania model surfaces. Pyruvic acid is chosen because the presence of a keto group adjacent to the acid functionality may change the adsorption behavior of monocarboxylic acids. Furthermore, pyruvic acid plays a prominent role in aquatic chemistry [30]. The suitability of the model metal-oxide surfaces is tested by comparing the adsorption behavior to that of a corresponding metal oxide powder.

ATR-IR Spectroscopy. The principle of ATR-IR spectroscopy [8] is illustrated in *Fig. 1* for multiple internal reflections and for a thin catalytic film. *Fig. 2* depicts the home-made ATR cell used for the *in situ* adsorption measurements described in the following. In contrast to transmission IR (T-FTIR) spectroscopy where the IR beam passes directly through the sample, in the ATR mode the IR radiation is coupled into the internal reflection element (IRE), an IR transparent crystal of high refractive index (n_1) in contact with the sample (n_2, with $n_1 > n_2$). The IR radiation propagates through the IRE at an angle of incidence (θ) larger than the critical angle, such that *total reflection* occurs at the IRE-sample interface. An evanescent electromagnetic field is

generated that penetrates into the sample and is *attenuated* by the sample, thus producing an IR spectrum. The amplitude of the electric field decays exponentially with the distance from the IRE. The penetration depth (d_p) is the distance from the interface where the intensity of the electric field falls to 1/*e* of its original value at the interface

$$d_p = \frac{\lambda_1}{2\pi\sqrt{\sin^2\theta - n_{21}^2}}$$

where $\lambda_1 = \lambda/n_1$ is the wavelength in the denser medium, λ the wavelength of the incoming radiation and $n_{21} = n_2/n_1$. The above equation holds for a two-phase system (IRE/sample) [8]. Typically, d_p is on the order of 1 μm. For bulk materials, the degree of coupling between the evanescent field and the absorbing sample is given by the effective thickness

$$d_e = \frac{n_{21}E_0^2 d_p}{2\cos\theta}$$

where E_0 is the amplitude of the electric field at the interface. The effective thickness expresses the equivalent path length in a hypothetical transmission measurement, which yields the same absorption as in an ATR experiment. The very short path length used in ATR-IR spectroscopy, implicit in d_e, makes this technique surface sensitive and, hence, suitable for the *in situ* characterization of heterogeneous catalysts. The sensitivity can be enhanced by using multiple reflection elements. The effective thickness depends on the refractive indices of IRE and sample. For example, by increasing or decreasing n_1 at constant λ_1 and n_2, d_e decreases or increases accordingly. Hence, by changing from Ge ($n_1 = 4.0$) to ZnSe ($n_1 = 2.4$), d_e increases, *i.e.*, more sample is probed by the IR radiation. Finally, the dependence of d_e on λ implies also that the intensity of the ATR signals increases with wavelength for bulk media and deviates from the intensity observed in a T-FTIR spectrum.

The simple equations given above were derived for a two-phase system [8]. In this work, we study the adsorption on thin films deposited on the IRE in contact with a solvent. Hence, we are dealing with at least a three-phase system IRE/film/solvent. For the case of a N-phase system of stratified optically isotropic media, general equations have been derived that describe its optical behavior [31]. The resulting equations are rather complex, and the underlying physics is not easily apparent. However, numerical calculations are readily performed. The calculations assume semi-infinite first and last layers, and nonabsorbing first layer. The reflectance R and electric field E of parallel and perpendicular polarized light are functions of the complex refractive indices and thickness of each layer as well as of the angle of incidence, and the wavelength of the radiation. The rate of energy dissipation, and, thus, the absorption of the IR light, is proportional to the mean-square electric field $\langle E^2 \rangle$, which is a function of wavelength and position. It is, therefore, important to know the mean-square electric fields as a function of the distance from the interface. *Fig. 3* shows a plot of the mean-square electric fields in the *x*, *y*, and *z* directions (see *Fig. 1*). The calculations were performed

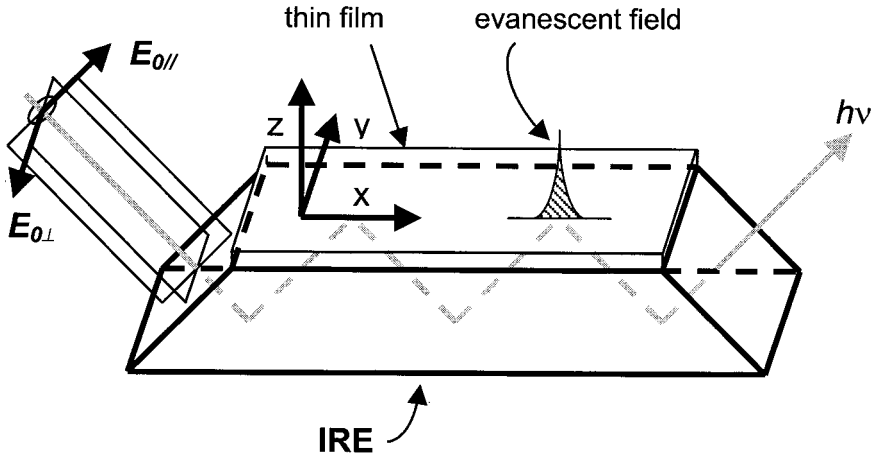

Fig. 1. *An attenuated total reflection setup allowing multiple internal reflections.* The IR beam propagates through the coated trapezoidal IRE and is totally reflected at the thin film-liquid interface. The electric field vectors for the parallel ($E_0\perp$) and perpendicular (E_0) polarized radiation and a Cartesian axes system on top of the thin film are also shown.

according to the equations derived by *Hansen* [31] and represent the system Ge IRE/100 nm Al_2O_3/CH_2Cl_2 solvent. It is apparent that the mean-square electric fields fall off steeply with the distance from the interface. The z component of the mean-square electric field is rather small within the IRE near the interface (small negative z) but is quite enhanced in the solution near the interface (small positive z). The presence of the Al_2O_3 film has only a small influence on the fields in the solution, as a calculation for the two-phase system Ge IRE/CH_2Cl_2 solution reveals (not shown).

Results and Discussion. – *Characterization of the Metal Oxide Layers.* Both XRD analysis of up to 1-μm thick Al_2O_3 films and determination of the refractive index ($n = 1.62$) of freshly deposited 100-nm Al_2O_3 by ellipsometry indicated that the vapor-deposited metal-oxide film is amorphous. Crystalline Al_2O_3 is characterized by a refractive index slightly higher than 1.7 [32]. The value obtained for n is in good agreement with previously reported data for films prepared by MOCVD [33], ion beam evaporation [34], and rf sputtering [35]. Amorphous surfaces were previously obtained by sputtering alumina on ZnSe ($n = 1.67$ [36]) and titania on Ge IREs [37]. In contrast, *Sperline et al.* assumed the optical properties of sputtered Al_2O_3 films to be identical to those of crystalline Al_2O_3 [38].

Fig. 4 shows an AFM image of the 100-nm thick Al_2O_3 layer together with the Al 2p, Ti 2p, C 1s and O 1s XP spectra for the Al_2O_3 and TiO_2 films. In the AFM image, the main feature is the net of scratches originating from polishing with diamond paste. The surface looks rather flat even though round particles of the size of 20 – 50 nm exhibiting different thickness can be observed. Since no signal of the underlying Ge IRE could be detected by XPS, it can be concluded that the films are continuous.

The XP spectra (*Fig. 4*) of both vapor-deposited metal-oxide films are close to reference materials. The singlet for Al at 74.9 eV ($2p_{3/2}$) is assigned to Al^{3+}, whereas the

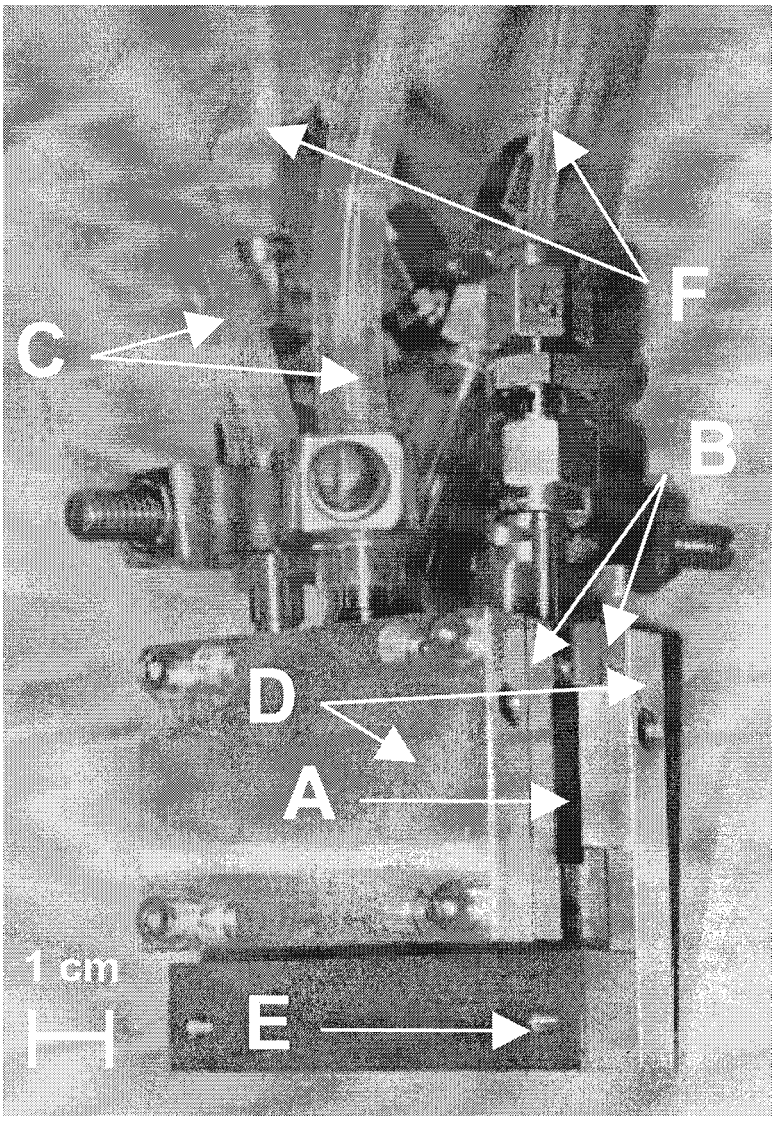

Fig. 2. *The home-made ATR-IR cell for* in situ *studies.* The picture shows the cell body (*A*) together with a Ge IRE (*B*) and the cooling system (*C*, water tubings and *D*, cooling jackets). *E* is the emplacement of the thermocouple. *F* is the in- and outlet of solutions to and from the cell.

doublet observed for Ti at 464.8 ($2p_{1/2}$) and 458.6 ($2p_{3/2}$) eV to Ti^{4+}. A shoulder on the high-energy side of the C signals (*ca.* 288 eV) more clearly visible for Al_2O_3 suggests the presence of carbonates, which represent *ca.* 11% of the C signal.

The oxide films did not significantly attenuate the IR light above 900 cm^{-1}. The most intense feature in the ATR spectra of vapor-deposited Al_2O_3 and TiO_2 is the envelope below 1000 cm^{-1}, displaying strong absorptions at *ca.* 846, 760, and 700 cm^{-1}.

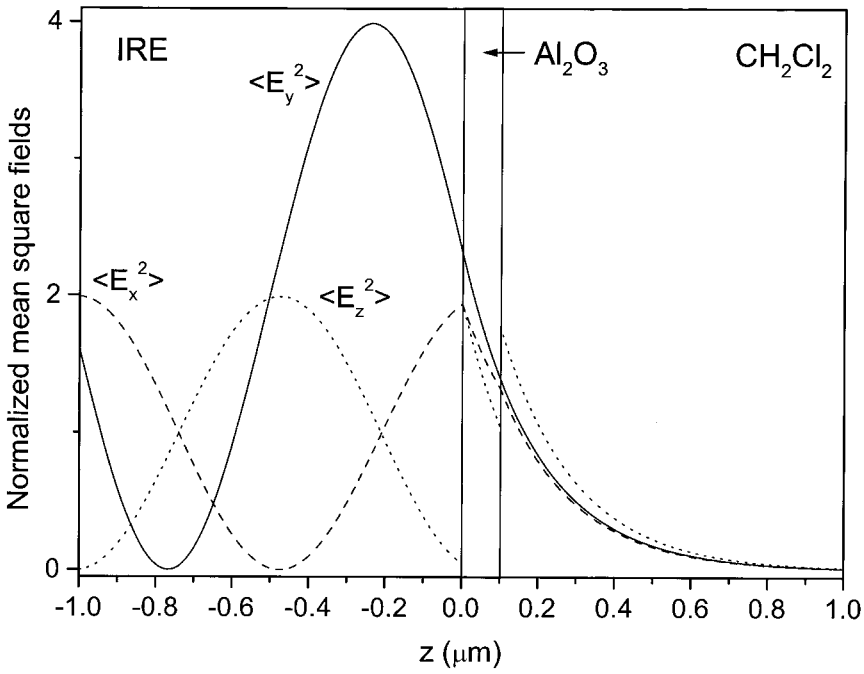

Fig. 3. *Calculated mean-square electric fields as a function of* z *for the system Ge internal reflection element* (n = *4.0)/100 nm* Al_2O_3 (n = *1.62)/*CH_2Cl_2 *solvent* (n = *1.42)*. The angle of incidence was 45°. Wavelength: 6 μm. The mean-square fields are normalized by taking the amplitude of the electric vectors of the incident fields in the first phase (Ge IRE) as unity. For the direction of *x*, *y*, and *z*, see *Fig. 1.*

Comparison with the typical absorptions of a neat Ge IRE showed that the three signals are characteristic of the Ge substrate [8]. An additional band, which is not characteristic of the neat materials [39], could be clearly distinguished at *ca.* 940 cm^{-1}. This signal has been reported for alumina layers obtained by MOCVD on AISI 304 steel but it is not assigned to a typical Al–O vibration [33][40][41]. The same band was also observed for Al_2O_3 layers obtained by low-power oxygen discharge [42]. A similar, though negative, band was reported for Cu thin films on Ge substrates and was assigned to the very thin layer of germanium oxide present on the bare Ge IRE [43]. This assignment is supported by the signal observed in mixed metal-oxides at 950 cm^{-1} corresponding to M–O–M′ vibrations [44].

In comparison to the vapor-deposited Al_2O_3 film, the α-Al_2O_3 layer did not exhibit the signal at 940 cm^{-1}. The typical Al–O vibration was clearly visible on Ge. Therefore, the signals observed in the ATR spectra of vapor-deposited alumina and titania at 940, 846, 760, and 700 cm^{-1} are assigned to germanium oxide and Ge. Upon deposition of the thin films the electric field due to the IR light is changed at the Ge/germanium oxide/thin film interface, leading to incomplete compensation of the absorptions due to the Ge and germanium oxide.

Careful inspection of the ATR spectra of vapor-deposited Al_2O_3 and TiO_2 also revealed weak signals due to adsorbed carbonate species in the 1650–1400 cm^{-1}

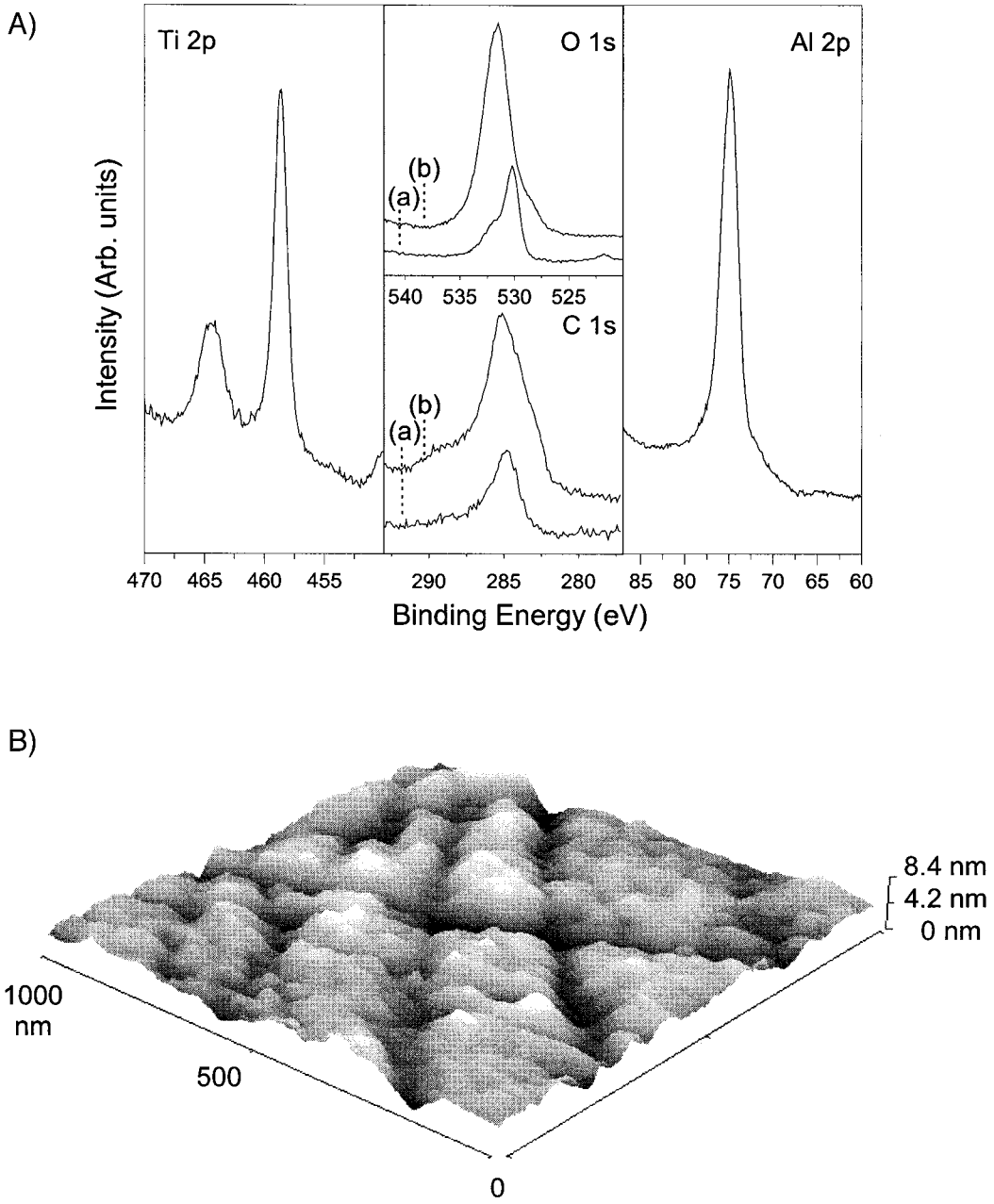

Fig. 4. A) *X-Ray photoelectron spectra of vapor-deposited Al_2O_3 and TiO_2 films showing the Al 2p, Ti 2p, C 1s and O 1s signals.* Traces *a* and *b* correspond to TiO_2 and Al_2O_3, respectively. B) *AFM Image of the Al_2O_3 film surface* (scan area 1 μm × 1 μm).

spectral region, in agreement with XPS data. A broad envelope in the 3700 – 3000 cm^{-1} spectral region indicated that the freshly vapor-deposited metal oxide surface was hydrated.

The thickness of the films measured before and after the adsorption measurements by ellipsometry indicated that the films are stable under the applied experimental conditions.

Adsorption of Formic and Acetic Acids. Fig. 5 shows the ATR spectra of a 0.01M solution of HCOOH in CH_2Cl_2 in contact with the vapor-deposited Al_2O_3 thin film. Signals of the asymmetric and symmetric COO stretching of formate species are clearly visible at 1606 and 1395 cm^{-1} ($\Delta_c = 211$ cm^{-1}) [45] together with the characteristic signals of dissolved HCOOH at 1743 and 1720 cm^{-1} (*Fig. 5, a*). Consistently, these last bands are completely attenuated by the following solvent flow, leaving only bands of surface formate species (*Fig. 5, b*).

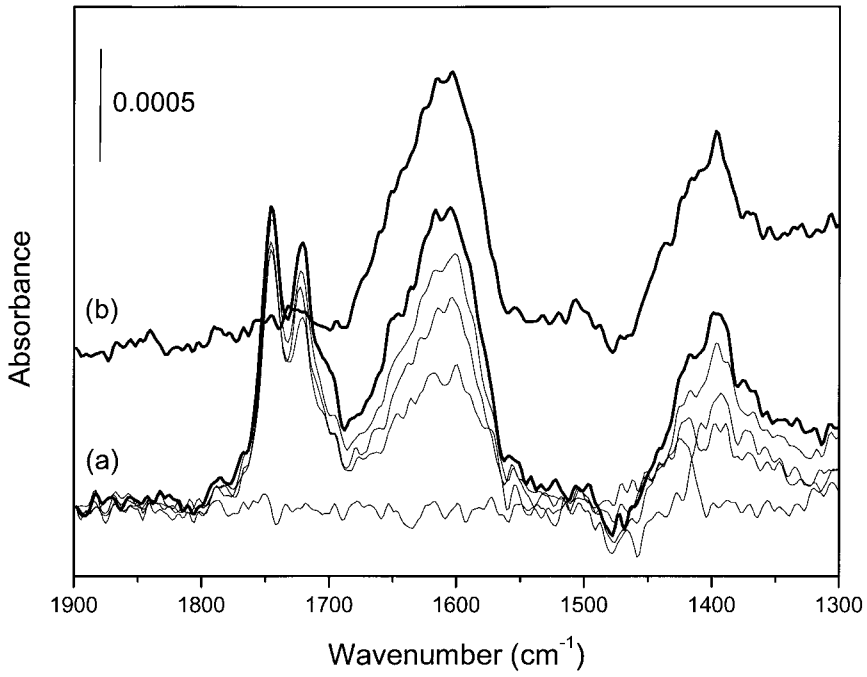

Fig. 5. ATR Spectra of HCOOH adsorbed on the vapor-deposited Al_2O_3 thin film from a 0.01M solution in CH_2Cl_2. Adsorption (*a*) and desorption (*b*) steps are shown.

When a 0.01M solution of CH_3COOH in CH_2Cl_2 contacted the vapor-deposited alumina film, two signals developed at 1569 and 1414 cm^{-1} ($\Delta_c = 155$ cm^{-1}) and indicated formation of acetate species [45]. Two signals were also observed at 1758 and 1712 cm^{-1} during CH_3COOH adsorption, which disappeared upon neat solvent flow and were assigned to dissolved CH_3COOH.

Adsorption of Pyruvic Acid. Compared to other common carboxylic acids, pyruvic acid (2-oxopropanoic acid; PA) poorly associates in solution. An intramolecular H-bond bridges the α-keto group to the acidic proton [46]. The stability of the *cis*

conformation of PA has been largely described in literature and refers to the position of the keto group relative to that of the OH [47–49]. *Table 1* summarizes the main vibrations of PA in CH_2Cl_2 and CCl_4 in the 1900–1600 cm^{-1} window. The signals observed at 1783 and 1728 cm^{-1} in CH_2Cl_2 are associated with the ν(C=O) of the free ester group ($\nu(C{=}O)_e$) and of the H-bonded α-keto group ($\nu(C{=}O)_k$), respectively. Two other signals observed at 1380 and 1347 cm^{-1} represent a combination band and the $\delta_s(CH_3)$. PA in CCl_4 exhibits the same, though slightly shifted, signals.

Table 1. *Vibrational Frequencies of PA and Pyruvate Ion.* The value for Δ_i is also given in the last entry.

PA		PA + Qd[a])		NaP[b])	NaP[c])	Assignment
CH_2Cl_2	CCl_4	CH_2Cl_2	CCl_4			
1783	1789					$\nu(C{=}O)_e$
1728	1724	1706	1714	1708	1709	$\nu(C{=}O)_k$
		1627	1627	1608	1633	$\nu_{AS}(COO)$
		n.o.	1421	1392	1405	$\nu_S(COO)$
1347	1346	1347	1346	1356	1353	$\delta_S(CH_3)$
			216	216	228	Δ_i

[a]) Values for $C_{PA} = C_{Qd} = 0.01$M; n.o.: not observed. [b]) Measured in aqueous solution in the ATR mode over the bare Ge crystal. [c]) Anhydrous, from [51].

Although keto-enol tautomerism is expected in the pyruvate ion, conformational analysis established that the most stable species in the liquid phase is the keto form [49]. Spectra of sodium pyruvate (NaP) are available for the solid phase (KBr wafer) and aqueous solutions. Since NaP is the main reference for recognizing adsorbed pyruvate species, ATR spectra of NaP in H_2O were recorded on the bare Ge crystal. The bands corresponding to the α-keto group, the asymmetric and (rather weak) symmetric O–C–O stretchings, and the umbrella mode of the Me group have been found at 1708, 1608, 1392, and 1353 cm^{-1}, respectively. A KBr wafer exhibited the following frequencies for the same group vibrations: 1708, 1631, 1405, and 1353 cm^{-1} in good agreement with previous data [50][51]. The difference in frequency between $\nu_{AS}(COO^-)$ and $\nu_S(COO^-)$, defined as Δ_i, is 216 and 228 cm^{-1} for NaP in the two phases, respectively.

The COO^- stretches of the pyruvate ion in aqueous solution have been reported at 1602 and 1395 cm^{-1} [52]. On the other hand, *Cabaniss* and *McVey* reported values of 1601 and 1356 cm^{-1} [45]. These values correspond to $\Delta_i = 207$ and 245 cm^{-1}, respectively. However, the second reference is in disagreement with all the reported data for the symmetric stretch of the pyruvate ion. The value of $\Delta_i = 207$ cm^{-1} well compares with the observed value for NaP in H_2O over the Ge IRE.

Since PA adsorption was studied in CH_2Cl_2 and CCl_4, quinuclidine (Qd) was added to PA, and the spectra were measured in these two solvents to obtain the spectrum of the pyruvate ion. The results are shown in *Fig. 6* and summarized in *Table 1*. The difference between the two solvents is only marginal. The COO^- asymmetric stretching exhibits the same frequency in both solvents, whereas a difference of only 1 cm^{-1} is observed for $\delta(CH_3)$. The shoulder at 1600 cm^{-1} observed in the case of CH_2Cl_2 is attributable to the COO^- group of a 1:2 base-acid complex [53]. In contrast, the

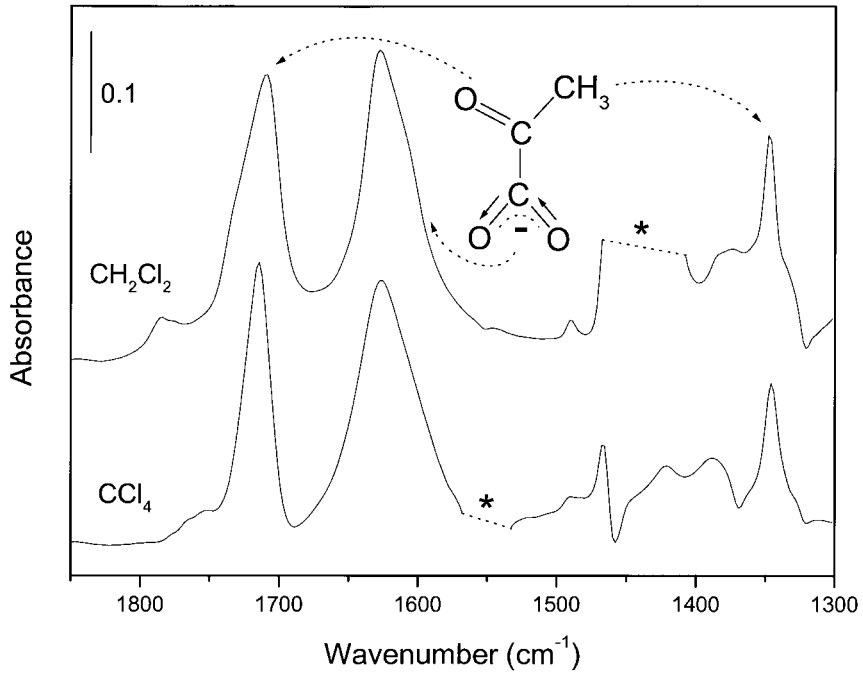

Fig. 6. *T-FTIR Spectra of PA-Qd solutions in CH_2Cl_2 and CCl_4.* The arrows indicate the vibrations of the pyruvate ion, whereas the asterisk represents solvent interference.

position of the α-keto-group vibration of the pyruvate ion is different in the two solvents. As shown in *Table 1*, it is found at 1706 cm^{-1} in CH_2Cl_2 and at 1714 cm^{-1} in CCl_4. Furthermore, the symmetric stretch ($\nu_S(COO^-)$) is clearly visible in CCl_4 (1421 cm^{-1}) but covered by strong solvent absorption in CH_2Cl_2. For analogy to ν_{AS}, it can be assumed similar in CCl_4 and CH_2Cl_2 leading to a value of 216 cm^{-1} for Δ_i.

The value of Δ can be used to determine the bonding mode of adsorbed pyruvate allowing the discrimination between mono- and bidentate geometry [54–56]. Briefly, if the metal-complexed species exhibits a Δ higher than that of the free ionic species (*i.e.*, $\Delta_c > \Delta_i$) the carboxylate is monodentate. This is the easiest species to recognize from the shift of the two COO^- stretches, since this shift is rather large. On the other hand, the discrimination between bidentate and bridging species is often difficult [54][55]. In these two cases $\Delta_c < \Delta_i$ and $\Delta_c \approx \Delta_i$, respectively. It must be noted that the magnitude of the shift between the two COO^- vibrations may be affected by the nature of the metal center and its polarizing effect [57].

This empirical rule has been extended to the adsorption of several organic acids on different metal oxides from aqueous solution [15][16][18–21][36][37][52][58–61].

Figs. 7 and *8* show ATR spectra of PA from a 0.01M solution in CH_2Cl_2 on vapor-deposited Al_2O_3 and TiO_2, respectively. Assignments are given in *Table 2*. Adsorption from CCl_4 did not exhibit any difference with respect to CH_2Cl_2. During PA adsorption, the 1900–1300 cm^{-1} spectral region displays signals of both adsorbed pyruvate and

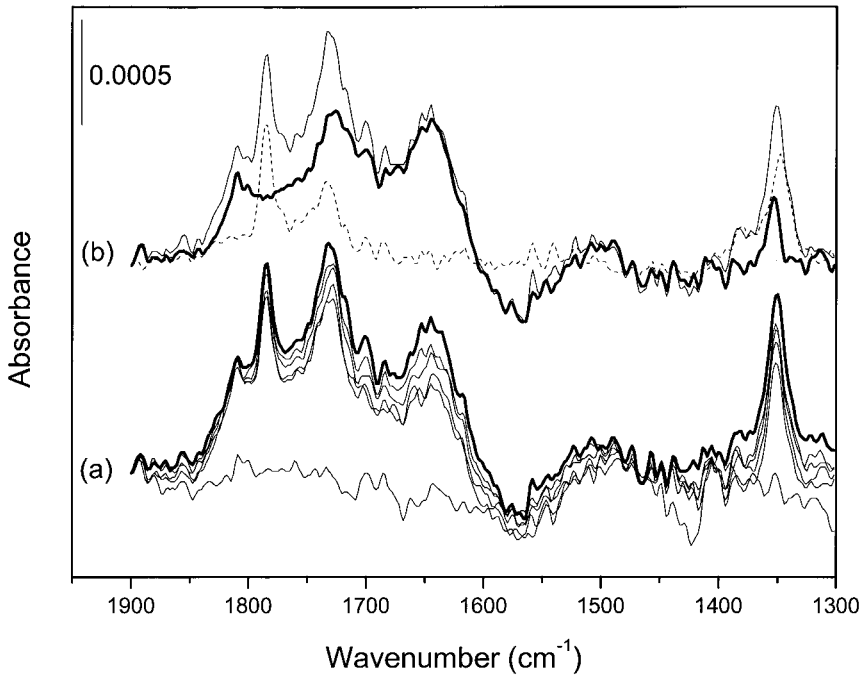

Fig. 7. *ATR Spectra of PA adsorbed on the vapor-deposited Al_2O_3 thin film from a 0.01*M *solution in CH_2Cl_2.* Adsorption (*a*) and desorption (*b*) steps are shown. The bold and dotted lines represent the last spectrum of each step and the difference between the two spectra, respectively.

Table 2. *PA Adsorption on Al_2O_3, TiO_2, and α-Al_2O_3 from CH_2Cl_2.* The values for Δ are also given. Values in parenthesis are referred to CCl_4 solvent. See *Results and Discussion* for further details.

PA				Assignment
Al_2O_3	TiO_2	α-Al_2O_3	Pa + Qd	
1727	1713	1727	1706	$\nu(C{=}O)_k$
1646	1630	1646	1627	$\nu_{AS}(COO^-)$
		1381	(1421)	$\nu_S(COO^-)$
1354	1355	1354	1347	$\delta_S(CH_3)$
			(216)	Δ_i
		265		Δ_c

dissolved PA on both metal oxides. The signals of dissolved PA disappear with a flow of neat solvent.

Adsorbed pyruvate on Al_2O_3 and TiO_2 is identified by the broad signal at 1646 and 1630 cm^{-1}, respectively, which is not found in the spectrum of PA. In analogy to *Fig. 6*, this signal is assigned to the asymmetric stretching of the COO^- group. There is apparently no trace of $\nu_S(COO^-)$ in the spectra of PA adsorbed over the vapor-deposited thin films, consistent with the very weak signals observed in the NaP sample and with the spectra of the pyruvate ion generated from PA and Qd in solution (*Fig. 6*).

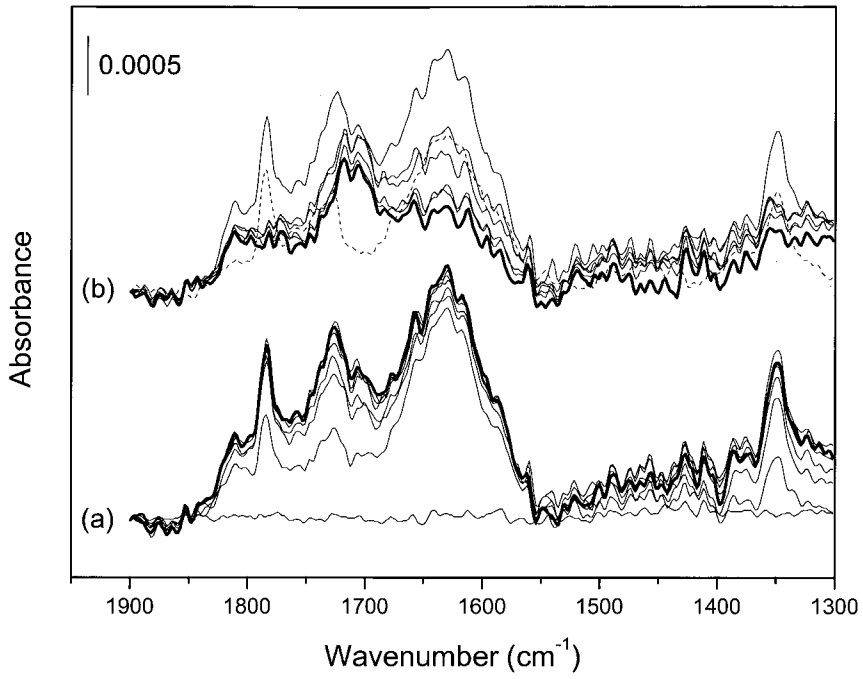

Fig. 8. *ATR Spectra of PA adsorbed on the vapor-deposited TiO_2 thin film from a 0.01*M *solution in CH_2Cl_2.* Adsorption (*a*) and desorption (*b*) steps are shown. The bold and dotted lines represent the last spectrum of each step and the difference between the two spectra, respectively.

Signals at *ca.* 1780 (sharp), 1730, and 1350 cm^{-1} on Al_2O_3 and TiO_2 belong to PA. The broadness of the signal at 1730 cm^{-1} indicates that more than one species may contribute to it. The dotted lines in *Figs.* 7 and *8* represent difference spectra obtained by subtracting the last spectrum during PA desorption from the last spectrum recorded during PA adsorption. The shoulder on the low frequency side of the signal at 1730 cm^{-1} can be detected already during adsorption particularly on TiO_2 (*Fig. 8*) and becomes clearly visible during the desorption step. The two difference spectra shown in *Figs. 7* and *8* also clearly show that the signal is composed of at least two bands. Similar behavior is observed for the signal at 1350 cm^{-1} ($\delta(CH_3)$), which is reduced in intensity upon the flow of solvent. The signal at 1780 cm^{-1} completely disappears during the desorption step, suggesting that it belongs to dissolved PA.

The difference spectrum in *Fig. 7* represents a spectrum of PA in solution. The absence of a band at *ca.* 1600 cm^{-1} and the close resemblance to a spectrum of dissolved PA indicate that no adsorbed pyruvate is removed from Al_2O_3 during neat solvent flow. *Fig. 8* shows that, in the case of TiO_2, both bands at 1713 and 1630 cm^{-1} decrease in intensity. The difference spectrum in *Fig. 8* exhibits the characteristic signals of dissolved PA and a substantial component of pyruvate species (broad band at *ca.* 1630 cm^{-1}). This suggests that at least part of the pyruvate ion is also removed by the solvent and, therefore, is less strongly adsorbed on titania than on alumina. However,

comparison of *Fig. 7* with *Fig. 8* shows that the intensity of the $\nu_{AS}(COO^-)$ signal is very similar for the two metal oxides.

Fig. 9 shows PA adsorption on the deposited α-Al_2O_3 powder. The main difference with adsorbed pyruvate on vapor-deposited Al_2O_3 is the appearance of the signal at 1381 cm^{-1} that is readily assigned to the symmetric stretching of the adsorbed carboxylate. Though less resolved, the signals on α-Al_2O_3 show the same position as on the vapor-deposited Al_2O_3 film indicating that the adsorption behavior of the acid is independent from the technique used to produce the adsorbent film.

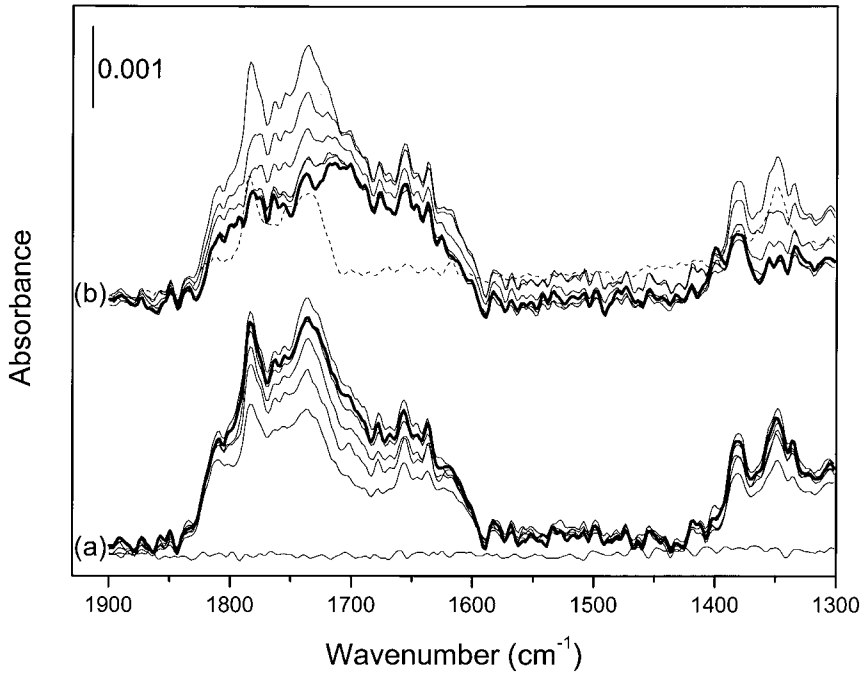

Fig. 9. *ATR Spectra of PA adsorbed on the deposited α-Al_2O_3 powder from a 0.01*M *solution in CH_2Cl_2.* Adsorption (*a*) and desorption (*b*) steps are shown. The bold and dotted lines represent the last spectrum of each step and the difference between the two spectra, respectively.

A common feature of adsorbed pyruvate on Al_2O_3 and TiO_2 is the signal of the α-keto group at 1727 and 1713 cm^{-1}, respectively. In contrast, no signal due to the α-keto group has been reported for PA on TiO_2 [52], where adsorption *via* both the COO^- and the keto groups has been proposed. However, a red shift of the keto C=O signal at *ca.* 1730 cm^{-1} rather would be expected on coordination of this functional group. On Al_2O_3, a signal was reported at 1760 cm^{-1} and assigned to the α-keto group of PA [42].

Under the present experimental conditions, the frequency of the α-keto group is located in between the frequencies of free PA and of the pyruvate ion (in CH_2Cl_2), as shown in *Table 2*. However, a difference exists between alumina and titania. A value close to that of neat PA is observed for Al_2O_3, with a shift of only 3 cm^{-1} with respect to the free acid, whereas, for TiO_2, the frequency is similar to that of the pyruvate ion, with a difference of 7 cm^{-1}. This suggests that the keto group interacts differently with the

two surfaces. The observed difference in the frequency of the α-keto group for the pyruvate adsorbed on alumina and titania is likely due to the different binding mode of the pyruvate ion to the metal oxide.

ATR Spectra of PA on Al_2O_3 and TiO_2 also display a signal at *ca.* 1810 cm^{-1}, which grows in with the pyruvate signals but does not disappear with dissolved PA. This signal has, therefore, to be assigned to a surface species, different from PA. The band is tentatively assigned to the $\nu(C{=}O)$ vibration of adsorbed PA dimers, since pyruvates and PA are known to dimerize [62–65]. These species could come directly from the solution or be the product of the surface reaction involving adsorbed pyruvate.

Structure of Adsorbed Species. The effect of the introduction of a functional group in the structure of a carboxylic acid on the adsorption behavior of the acid is depicted in *Fig. 10* for the series formic acid (C_1), acetic acid (C_2), and PA (C_3). The present results indicate that changes in the coordination mode of the acid to the Al_2O_3 surface occur on introduction of a keto group adjacent to the carboxy moiety.

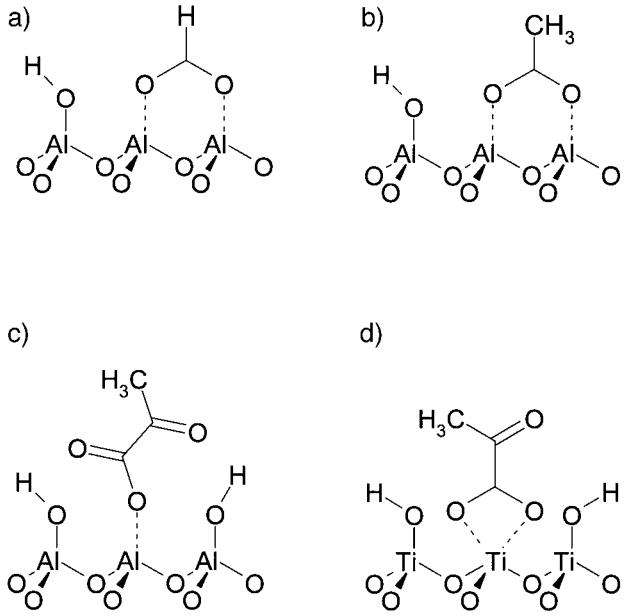

Fig. 10. *Proposed structure of main surface species resulting from adsorption of carboxylic acids dissolved in CH_2Cl_2. a*) HCOOH adsorption on alumina, *b*) CH_3COOH adsorption on alumina, *c*) pyruvic acid adsorption on alumina, *d*) pyruvic acid adsorption on titania.

According to the values of Δ_c found for HCOOH and CH_3COOH, and the values of Δ_i for aqueous solutions of sodium formate and acetate ($\Delta_i = 229$ and 135 cm^{-1}, respectively [45]), it is proposed that these two acids adsorb on the alumina surface forming formate and acetate species, which interact with both O-atoms of the carboxylate group. The small difference between Δ_c and Δ_i would indicate a bridging structure in both cases, which is shown in *Fig. 10*. However, a bidentate species cannot be ruled out, particularly for formate, where $\Delta_c < \Delta_i$. Hence, the substitution of the H-atom with the CH_3 group does not considerably influence the adsorption mode of the

acid. Similar behavior is known for adsorption of HCOOH and CH_3COOH at solid-gas interfaces [66][67].

The orientation of adsorbed pyruvate on the two metal oxides can also be tentatively deduced from the values of Δ. The proposed structures are shown in *Fig. 10*. Since both the vapor-deposited Al_2O_3 and the α-Al_2O_3 films give identical frequencies for the stretchings of the α-keto and the COO^- group (asymmetric stretching), the value of $\nu_S(COO^-)$ is assumed similar for both oxides. This leads to $\Delta_c = 265\ cm^{-1}$. As previously shown $\Delta_i = 216\ cm^{-1}$ is the value obtained with PA and Qd in solution (*Table 1*). The difference between the two values is then $49\ cm^{-1}$, suggesting that PA exhibits predominantly monodentate species on alumina. Some degree of H-bonding with the surface OH groups may be invoked to explain the origin of the frequency of the α-keto group of adsorbed pyruvate, although the difference with free PA is only marginal. The frequency of the α-keto group could also suggest that the adsorbed species on alumina is close to an α-keto ester [68], which again supports the monodentate binding mode. The assignment is in good agreement with the binding mode of CH_3COOH [69], salicylic acid [15], and sodium laurate [36] over the same metal oxide, although the value of Δ_c is in contrast to that previously reported of $216\ cm^{-1}$ [42]. The different experimental conditions are probably at the origin of the discrepancy.

Since the asymmetric stretching of the COO^- group of adsorbed pyruvate on TiO_2 is similar to the one observed with PA and Qd, the surface species on TiO_2 should exhibit a value for $\nu_S(COO^-)$ close to that observed for the pyruvate ion. With the assumption that $\Delta_c \approx \Delta_i$, it is, however, difficult to discriminate between bridging and bidentate species. A bidentate species can be tentatively proposed. In recent adsorption studies of a number of carboxylic acids [20][52][60][61][70–72], TiO_2 has been reported to bind two O-atoms, independently from the presence of an additional functional group (*e.g.*, OH) in the adsorbate. This is in agreement with the presence of Ti^{4+} ions allowing the coordination to more than one O atom, in contrast to alumina.

It cannot be excluded that the α-keto group interacts with the OH groups of the surface. However, the frequency of this group on the TiO_2 is almost identical to that of the pyruvate ion (compare *Table 2* with *Table 1*). The monodentate species observed for Al_2O_3 does not force the molecule in a fixed position allowing H-bonding, *i.e.*, further interaction with the hydrated surface (*Fig. 10*). On the other hand, on TiO_2 the α-keto group points away from the surface and appears close to the α-keto group of a free pyruvate ion.

Conclusions. – The adsorption of various carboxylic acids (HCOOH, CH_3COOH, and pyruvic acid) on vapor-deposited alumina and titania films as well as on a layer of α-Al_2O_3 powder has been studied by *in situ* ATR-IR. Adsorption of HCOOH and CH_3COOH on Al_2O_3 afforded mainly bridging formate and acetate species, similarly as observed when these acids are adsorbed from the gas phase on this material. Pyruvic acid also adsorbs mainly through the COO^- group on both metal-oxide surfaces. However, the presence of the keto group in α-position allows another interaction, *i.e.*, with the surface OH groups. The adsorption involves the coordination of the pyruvate ion to a metal center, revealing surface defects in the metal-oxide film. Two distinct adsorption modes of pyruvic acid on alumina and titania have been observed. A

monodentate complex is found for alumina, whereas bidentate chelation is more likely for titania. A fraction of the adsorbed pyruvic acid was desorbed from the titania film by a flow of neat solvent, whereas no attenuation of the signals due to the pyruvate species was observed on alumina.

The thin film metal oxide surfaces proved to be suitable models to mimic the surface properties of corresponding metal-oxide powders.

Experimental Part

Materials. Pyruvic acid (*Fluka*, $\geq 98\%$) stored at 4°, HCOOH (*Fluka*, $\geq 98\%$), CH_3COOH (*Riedel-de H"en*, $> 99.8\%$), and quinuclidine (*Fluka*, $\geq 97\%$) were used as received. CH_2Cl_2 (*Baker*) and CCl_4 (*Merck*) were stored over 5-Å molecular sieves.

Preparation and Characterization of the Vapor-Deposited MO_z Films. The internal reflection element (IRE) was coated with 100 nm of MO_x (M = Al, Ti) by electron-beam physical vapor deposition as described in [9]. Spectra of freshly deposited thin films were obtained in the ATR mode. For this purpose, the coated IRE was mounted on a home-made PVDF holder.

X-Ray diffraction (XRD), X-ray photoelectron spectroscopy (XPS), and atomic force microscopy (AFM) were performed on the MO_x-coated Ge fragments (*ca.* 1 cm^2). XRD Analysis was carried out for the alumina thin films (up to 1-μm thickness) with a *Siemens D5000* diffractometer with CuK_α ($\lambda = 1.5148$ Å) radiation.

XPS Measurements of Al_2O_3 and TiO_2 thin films were performed on a *Leybold Heraeus LHS11* apparatus. X-Rays were generated by a Mg source (1253.6 eV) operating at 240 W. The spectrometer energy scale was calibrated using the Au $4f_{5/2}$, Ag $3d_{5/2}$, and Cu $2p_{3/2}$ lines at 84.2, 367.9, and 932.4 eV. Spectra were recorded at constant pass energy of 31.5 eV.

The morphology of the Al_2O_3 film was investigated by AFM with a commercial microscope (*TopoMetrix TMX2000*) operating in air and with pyramidal silicon nitride tips (*TopoMetrix*). For each sample, different areas were imaged to obtain representative information on the structure of the films. The structural features were, however, not sensitive to the area imaged.

Before and after PA adsorption on vapor-deposited Al_2O_3, the thickness and the refractive index of the metal-oxide layer were checked with a *Plasmos SD 2300* ellipsometer at a wavelength of 6328 Å and at an angle of incidence of 70° with a He-Ne laser.

Transmission IR (T-FTIR) spectra of solns. were recorded by means of a CaF_2 cell equipped with a 1-mm *Teflon* spacer.

Preparation of the α-Al_2O_3 Layer. Commercial α-Al_2O_3 (*Fluka*, *ca.* 98%) was ground in a mortar and sonicated for *ca.* 1 h in distilled H_2O. The suspension was then pipetted on the Ge IRE and allowed to evaporate in air overnight. Most of the thick layer was then removed by gentle cleaning with CH_2Cl_2.

Adsorption Studies. In situ ATR-IR measurements were carried out with the home-built flow-through stainless steel cell shown in *Fig. 2*, which was built following the design of *Fringeli* [73]. After preparation of the thin films, the coated IRE was mounted within the walls of the cell and fixed by means of two viton o-rings on the side on which the soln. was admitted and one viton o-ring on the other side. The gap between the IRE and the cell wall was 200 – 300 μm. Two water-cooled jackets have been fixed on the two sides of the ATR cell to control the temp., which was measured with a thermocouple positioned on the bottom part of the cell.

A commercial trapezoidal 45° 52 × 20 × 2 mm Ge IRE (*Graseby Specac*, 25 reflections) has been used. The transparent window for Ge extends between 5500 and 600 cm^{-1} in the IR region. However, absorptions due to the o-rings (weak) and the deposited materials (very strong) can dramatically alter the usable range. On the other hand, the relatively high value of the refractive index ($n = 4.0$) makes Ge a very good material for studying processes occurring at surfaces. All *in situ* ATR-IR spectra have been recorded on a *Bruker IFS-66* spectrometer equipped with a liquid N_2-cooled medium band MCT (HgCdTe) photodetector with a commercial ATR-IR unit (*Wilks Scientific*). Typically, spectra were obtained by accumulating 200 scans at 4 cm^{-1} resolution. The experiments were performed with unpolarised light. All spectra are presented in absorbance units as $A = -\log(I/I_0)$, where I and I_0 are the reflected intensity of the sample and reference, respectively. Since only one side of the ATR crystal is coated with a thin film, and the cell does not cover the whole crystal, only *ca.* 8 reflections are active.

Solns. were allowed to flow through the cell by means of a microdosing pump (*MDP-2*, *Saphirwerk Industrieprodukte*) at 1.7 ml/min. Solvent and solns. were stored in separate reservoirs equipped with glass frits

where they could be saturated with a gas. Three-ways PTFE manual valves allowed switching between the reservoirs.

After mounting the ATR element in the cell and alignment, the probe chamber was purged with dried air overnight in order to minimize signals of atmospheric CO_2 and H_2O. Before admission of CH_2Cl_2 or CCl_4, the reference spectrum, *i.e.*, MO_x (M = Al and Ti) over Ge, was recorded. Solvent saturated with N_2 (*PANGAS*, 99.995 vol %) was circulated through the cell until stabilization of the signal (*ca.* 2 h) had been reached. Then, a 0.01M soln. of the acid saturated with N_2 was circulated through the cell, followed by the desorption step consisting of a flow of N_2-saturated solvent. The last spectrum before admission of the acid was subtracted from all the spectra recorded during adsorption and desorption in order to obtain spectra of surface species. Where needed, signals from the H_2O gas-phase spectrum in the 1700 – 1400 cm^{-1} range have been subtracted.

The authors gratefully acknowledge Prof. Dr. *U. Fringeli* for valuable discussions, *P. Steiner* for manufacturing the cell, and the financial support of ETH-Zurich.

REFERENCES

[1] N. Sheppard, *Annu. Rev. Phys. Chem.* **1988**, *39*, 589.
[2] Y. J. Chabal, *Surf. Sci. Rep.* **1988**, *8*, 211.
[3] J. Ryczkowski, *Catal. Today* **2001**, *68*, 263.
[4] J. O'M. Bockris, S. U. M. Kahn, 'Surface Electrochemistry: A Molecular Level Approach', Plenum Press, New York, 1993.
[5] Y. R. Shen, *Annu. Rev. Phys. Chem.* **1989**, *40*, 327.
[6] T. Buffeteau, B. Desbat, J. M. Turlet, *Appl. Spectrosc.* **1991**, *45*, 380.
[7] M. Moskovits, *Rev. Mod. Phys.* **1985**, *57*, 783.
[8] N. J. Harrick, 'Internal Reflection Spectroscopy', Interscience Publishers, New York, 1967.
[9] D. Ferri, T. Bürgi, A. Baiker, *J. Phys. Chem. B* **2001**, *105*, 3187.
[10] D. Ferri, T. Bürgi, A. Baiker, *Chem. Commun.* **2001**, 1172.
[11] D. Ferri, T. Bürgi, *J. Am. Chem. Soc.* **2001**, *123*, 12074.
[12] T. Bürgi, *Phys. Chem. Chem. Phys.* **2001**, *3*, 2124.
[13] D. Ferri, T. Bürgi, Baiker, *J. Catal.* **2002**, *210*, 160.
[14] D. Ferri, T. Bürgi, A. Baiker, *Phys. Chem. Chem. Phys.* **2002**, *4*, 2667.
[15] M. V. Biber, W. Stumm, *Environ. Sci. Technol.* **1994**, *28*, 763.
[16] J. D. Kubicki, L. M. Schroeter, M. J. Itoh, B. N. Nguyen, S. E. Apitz, *Geochim. Cosmochim. Acta* **1999**, *63*, 2709.
[17] K. D. Dobson, A. J. McQuillan, *Spectrochim. Acta, Part A* **2000**, *56*, 557.
[18] M. I. Tejedor-Tejedor, E. C. Yost, M. A. Anderson, *Langmuir* **1990**, *6*, 979.
[19] M. I. Tejedor-Tejedor, E. C. Yost, M. A. Anderson, *Langmuir* **1992**, *8*, 525.
[20] S. J. Hug, B. Sulzberger, *Langmuir* **1994**, *10*, 3587.
[21] K. D. Dobson, A. J. McQuillan, *Spectrochim. Acta, Part A* **1999**, *55*, 1395.
[22] C. H. Specht, F. H. Frimmel, *Phys. Chem. Chem. Phys.* **2001**, *3*, 5444.
[23] E. M. Cordi, J. L. Falconer, *J. Catal.* **1996**, *162*, 104.
[24] G. Centi, *J. Mol. Catal. A: Chemical* **2001**, *173*, 287.
[25] W. Stumm, J. Morgan, 'Aquatic Chemistry', John Wiley & Sons, New York, 1981.
[26] P. H. Tewari, 'Adsorption from Aqueous Solution', Plenum Press, New York, 1981.
[27] M. Grätzel, 'Heterogeneous Photochemical Electron Transfer', CRC, Boca Raton, FL, 1989.
[28] 'Aquatic Surface Chemistry: Chemical Processes at the Particle-Water Interface', Ed. W. Stumm, John Wiley & Sons, New York, 1987.
[29] J. Wambach, A. Baiker, A. Wokaun, *Phys. Chem. Chem. Phys.* **1999**, *1*, 5071.
[30] B. Deng, A. T. Stone, *Environ. Sci. Technol.* **1996**, *30*, 2484.
[31] W. N. Hansen, *J. Opt. Soc. Am.* **1968**, *58*, 380.
[32] 'Handbook of Laser Science and Technology, Vol. 4: Optical Materials: Part 2', Ed. M. J. Weber, CRC Press, Boca Raton, 1986, IV Vol.
[33] V. A. C. Haanappel, H. D. van Corbach, T. Fransen, P. J. Gellings, *Surf. Coat. Technol.* **1994**, *63*, 145.
[34] M. Tan, S. I. Tan, Y. Shen, *IEEE Trans. Magn.* **1995**, *31*, 2694.
[35] B. J. H. Stadler, M. Oliveira, L. O. Bouthillette, *J. Am. Ceram. Soc.* **1995**, *78*, 3336.
[36] A. Couzis, E. Gulari, *Langmuir* **1993**, *9*, 3414.

[37] J. Drelich, Y. Lu, L. Chen, J. D. Miller, S. Guruswamy, *Appl. Surf. Sci.* **1998**, *125*, 236.
[38] R. P. Sperline, Y. Song, H. Freiser, *Langmuir* **1992**, *8*, 2183.
[39] C. Morterra, G. Magnacca, *Catal. Today* **1996**, *27*, 497.
[40] V. A. C. Haanappel, H. D. van Corbach, T. Fransen, P. J. Gellings, *Surf. Coat. Technol.* **1995**, *72*, 13.
[41] V. A. C. Haanappel, D. v.d. Vendel, H. D. van Corbach, T. Fransen, P. J. Gellings, *Thin Solid Films* **1995**, *256*, 8.
[42] S. Devdas, R. R. Mallik, R. Coast, P. N. Henriksen, *Surf. Sci.* **1995**, *326*, 327.
[43] K. P. Ishida, P. R. Griffiths, *Anal. Chem.* **1994**, *66*, 522.
[44] R. Neumann, M. Chava, M. Levin, *Chem. Commun.* **1993**, 1685.
[45] S. E. Cabaniss, I. F. McVey, *Spectrochim. Acta, Part A* **1995**, *51*, 2385.
[46] M. A. Abramovich, I. M. Ginzburg, D. V. Ioffe, *J. Gen. Chem. USSR (Eng. Translation)* **1974**, *44*, 2221.
[47] M. S. Gordon, D. E. Tallman, *Chem. Phys. Lett.* **1972**, *17*, 385.
[48] J. Murto, T. Raaska, H. Kunttu, M. Räsänen, *J. Mol. Struct.* **1989**, *200*, 93.
[49] K. E. Norris, J. E. Gready, *J. Mol. Struct.* **1992**, *258*, 109.
[50] D. A. Long, W. O. George, *Trans. Faraday Soc.* **1960**, *56*, 1570.
[51] M. Kakihana, M. Okamoto, *J. Phys. Chem.* **1984**, *88*, 1797.
[52] T. Awatani, K. D. Dobson, A. J. McQuillan, B. Ohtani, K. Uosaki, *Chem. Lett.* **1998**, 849.
[53] D. Ferri, T. Bürgi, A. Baiker, *J. Chem. Soc., Perkin Trans. 2* **1999**, 1305.
[54] G. B. Deacon, R. J. Phillips, *Coord. Chem. Rev.* **1980**, *33*, 227.
[55] R. C. Mehrotra, R. Bohra, 'Metal Carboxylates', Academic Press, New York, 1983, 48.
[56] K. Nakamoto, 'Infrared and Raman Spectra of Inorganic and Coordination Compounds', John Wiley & Sons, New York, 1986, 231.
[57] G. Busca, V. Lorenzelli, *Mater. Chem.* **1982**, *7*, 89.
[58] S. Hayashi, T. Takenaka, R. Gotoh, *Bull. Inst. Chem. Res.* **1969**, *47*, 378.
[59] E. C. Yost, M. I. Tejedor-Tejedor, M. A. Anderson, *Environ. Sci. Technol.* **1990**, *24*, 822.
[60] S. Tunesi, M. A. Anderson, *Langmuir* **1992**, *8*, 487.
[61] G. N. Ekstr"m, A. J. McQuillan, *J. Phys. Chem. B* **1999**, *103*, 10562.
[62] M. A. W. K. de Jong, *Recl. Trav. Chim. Pays-Bas* **1901**, *20*, 81.
[63] C. M. Montgomery, J. L. Webb, *Science* **1954**, *120*, 843.
[64] C. M. Montgomery, J. L. Webb, *J. Biol. Chem.* **1956**, *221*, 359.
[65] D. Ferri, T. Bürgi, K. Borszeky, T. Mallat, A. Baiker, *J. Catal.* **2000**, *193*, 139.
[66] J. M. Trillo, G. Munuera, J. M. Criado, *Catal. Rev.* **1972**, *7*, 51.
[67] J. Najbar, R. P. Eischens, in 'Proceedings of the 9th International Congress on Catalysis', Ed. M. J. Phillips, M. Ternan, 1988, Vol. 3, 1434.
[68] D. Ferri, T. Bürgi, A. Baiker, *J. Chem. Soc., Perkin Trans. 2* **2000**, 221.
[69] J. D. Kubicki, G. A. Blake, S. E. Apitz, *Geochim. Cosmochim. Acta* **1997**, *61*, 1031.
[70] S. T. Martin, J. M. Kesselman, D. S. Park, N. S. Lewis, M. R. Hoffmann, *Environ. Sci. Technol.* **1996**, *30*, 2535.
[71] N. W. Duffy, K. D. Dobson, K. C. Gordon, B. H. Robinson, A. J. McQuillan, *Chem. Phys. Lett.* **1997**, *266*, 451.
[72] A. Vittadini, A. Selloni, F. P. Rotzinger, M. Grätzel, *J. Phys. Chem. B* **2000**, *104*, 1300.
[73] U. P. Fringeli, in 'Internal Reflection Spectroscopy: Theory and Application', Ed. F. M. Mirabella, Marcel Dekker Inc., New York, 1992, 255.

Received June 3, 2002